
ELECTROMAGNETIC APPLICATIONS
IN BIOLOGY AND MEDICINE

LaserBreeze Gas Analyzer for Noninvasive Diagnostics
of Air Exhaled by Patients

A. A. Karapuzikov^{1*}, I. V. Sherstov^{1,2**}, D. B. Kolker^{2,3***},
A. I. Karapuzikov^{1****}, Yu. V. Kistenev^{4,5*****}, D. A. Kuzmin⁵,
M. Yu. Shtyrov¹, N. Yu. Dukhovnikova^{1,3*****}, K. G. Zenov¹, A. A. Boyko^{1,3},
M. K. Starikova^{1*****}, I. I. Tikhonyuk¹, I. B. Miroshnichenko^{1,3},
M. B. Miroshnichenko¹, Yu. B. Myakishev², and V. N. Lokonov^{2*****}

¹Special Technologies Ltd., ul. Zelenaya Gorka 1/3, Novosibirsk, 630060 Russia

²ISC OCTAVA, Krasnyi pr. 220, Novosibirsk, 630049 Russia

³Novosibirsk State Technical University, pr. Karla Marksa 20, Novosibirsk, 630092 Russia

⁴Tomsk State University, pr. Lenina 36, Tomsk, 634050 Russia

⁵Siberian State Medical University, Moskovskiy Trakt 2, Tomsk, 634050 Russia

Received April 15, 2014

Abstract—A laser gas analyzer has been designed for determining the composition of exhaled air by means of photoacoustic spectroscopy. The analyzer, based on a broadband optical parametric oscillator and photoacoustic detector, provides high-precision rapid analysis of the multicomponent composition of human exhaled air for dynamic estimation of the efficiency of treating bronchus and lung diseases.

DOI: 10.3103/S1541308X14030054

1. INTRODUCTION

Detection of volatile compounds (VCs) in exhaled air is an urgent and promising approach to develop new analytical and diagnostic methods in medicine [1–4]. The informativeness of analysis significantly increases with an increase in the content of detected VCs. A number of spectral instruments, aimed at solving diagnostic problems, are commercially produced. Their main drawback is the narrow working spectral range and, correspondingly, a small number of detectable gases. A LaserBreeze laser gas analyzer (hardware-software package), based on a broadband optical parametric oscillator and photoacoustic detector has been developed to solve this problem.

*E-mail: alexey.karapuzikov@gmail.com

**E-mail: sherstov@laser.nsc.ru

***E-mail: kolker@ngs.ru

****E-mail: ir@laser.nsc.ru

*****E-mail: yuk@iao.ru

*****E-mail: nduhovnikova@gmail.com

*****E-mail: starikova.mk@mail.ru

*****E-mail: lokonov@ngs.ru

2. DESIGN

The principle of LaserBreeze operation is based on laser photoacoustic spectroscopy (LPAS) [5]. Optical parametric oscillator (OPO) is used as a laser radiation source which provides radiation wavelength tuning in the spectral range from 2.5 to 11 μm [6]. The LaserBreeze appearance is shown in Fig. 1.

The main components of LaserBreeze are sample preparation unit (SPU), electronic control unit (ECU), optical unit, and stabilized power supply.

A bacterial filter is installed at the SPU input to collect dust and aerosol particles in a sample. To reduce the interfering background of water vapor absorption, a sample was previously placed in a freezing chamber to reduce humidity to 0.1 g m^{-3} .

The ECU is used to measure the photoacoustic detector (PAD) resonant frequency; set a desired repetition frequency and energy of pump laser pulses, a position of the channel selector, working temperatures of OPO-1 and OPO-2 nonlinear crystals, and desired OPO-1 and OPO-2 radiation wavelengths; process output signals from PAD, photodetector, and reference cell; and switch on/off SPU pump and valves.

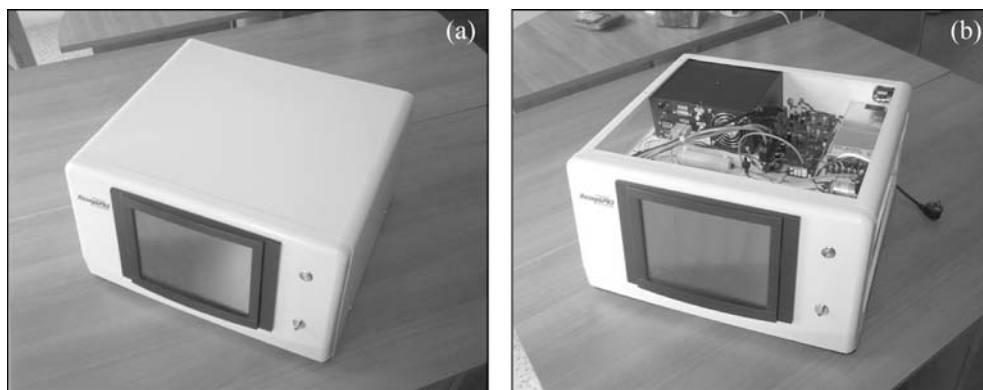


Fig. 1. External appearance of (a) ready-assembled LaserBreeze and (b) LaserBreeze without housing.

The controller is used to operate the motorized linear platform of OPO-1 and OPO-2, rotational platform of OPO-2, linear platform of channel selector, OPO-1 and OPO-2 thermostats, and SPU air pumps and valves.

The analog-digital converter is aimed at digitizing output signals of PAD, photodetector, and reference cell and supplying test voltage pulses to the PAD piezoelectric transducer during resonant frequency measurements.

The LaserBreeze optical unit (Fig. 2) consists of pump laser, OPO-1, OPO-2, channel selector, PAD, photodetector, reference cell, and optical-channel elements (lens, mirrors, etc.).

OPO-1 and OPO-2 are optically pumped by a Nd:YLF laser at a wavelength of $1.053\ \mu\text{m}$. The OPO-1 active element consists of two fan-out

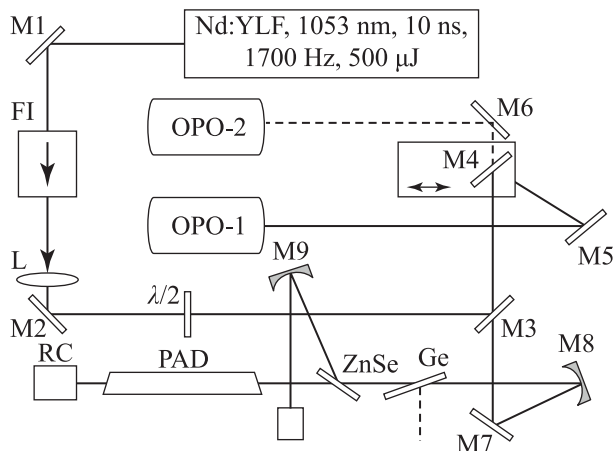


Fig. 2. LaserBreeze optical unit: (Nd:YLF) pump laser, (M1–M9) mirrors, (FI) Faraday isolator, (L) lens ($f = 200\ \text{mm}$), ($\lambda/2$) half-wave plate, (OPO-1) optical parametric oscillator based on a fan-out MgO:PPLN structure, (OPO-2) optical parametric oscillator based on HgGa₂S₄ crystals, (Ge) Ge plate, (ZnSe) ZnSe plate, (PED) pyroelectric detector, (PAD) photoacoustic detector, and (RC) reference cell.

MgO:PPLN structures, which make it possible to tune the wavelength in the range from 2.5 to $4.5\ \mu\text{m}$. OPO-2 is tuned in the range from 4 to $11\ \mu\text{m}$ due the total rotation of HgGa₂S₄ (HGS) crystals with respect to the optical axis and as a result of precise transverse displacement of two crystals with respect to the OPO cavity axis.

Figure 3(a) presents dependence of the pulse energy on wavelength of OPO-1. One can see that this energy decreases with an increase in wavelength, which can be explained by enhanced absorption in the PPLN structures. The highest OPO-1 pulse energy (to $38\ \mu\text{J}$) was observed at a wavelength close to $2.5\ \mu\text{m}$, whereas at the wavelength $\lambda = 4.0\ \mu\text{m}$ the pulse energy decreased to $2\text{--}3\ \mu\text{J}$.

Figure 3(b) presents the wavelength dependence of the average OPO-1 power. The pulse-repetition frequency was $1750\ \text{Hz}$, which corresponded to the current PAD resonant frequency. It can be seen that the wavelength dependence for the average power practically repeats the corresponding dependence for the OPO-1 pulse energy. The largest average OPO-1 power (about $70\ \text{mW}$) was obtained at the wavelength $\lambda = 2.5\ \mu\text{m}$. With an increase in wavelength, the average radiation power monotonically decreased to $10\text{--}15\ \text{mW}$ at the wavelength $\lambda = 3\text{--}3.8\ \mu\text{m}$; this behavior is in good agreement with the previous results.

Figure 4(a) shows wavelength dependences for the OPO-2 pulse energy (two curves, corresponding to crystals #1 and #2). One can see that the pulse energy for crystal #1 reaches maximum values of about $4.4\ \mu\text{J}$ at the wavelength $\lambda = 5.2\ \mu\text{m}$. The pulse energy for crystal #2 monotonically decreases with an increase in wavelength, which can be explained by the enhanced absorption in HGS crystals at longer wavelengths. Note that the lasing on HGS crystals in the nanosecond mode in the spectral range from 8 to $11\ \mu\text{m}$ was obtained by us for the first time [7]. The highest pulse energy (to $4.5\ \mu\text{J}$) for OPO-2

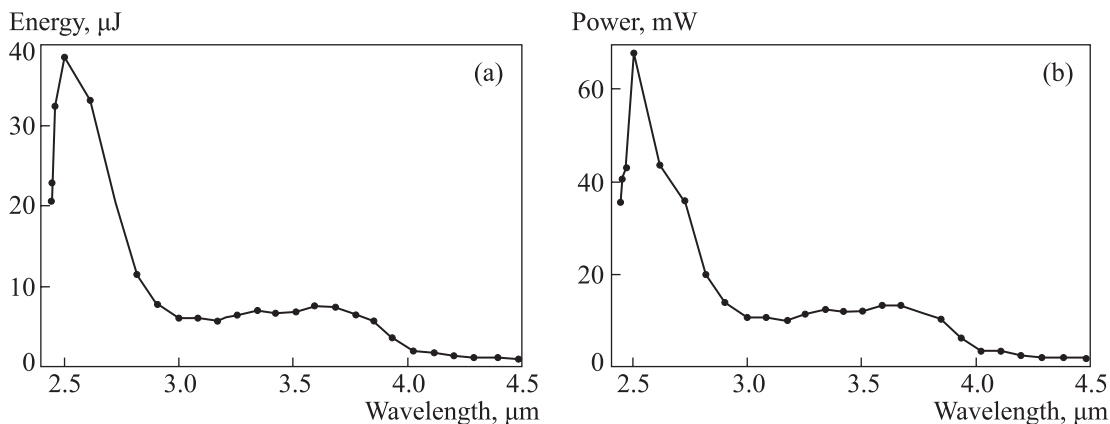


Fig. 3. Dependences of the (a) pulse energy and (b) average power on wavelength of OPO-1; the pulse-repetition frequency is 1750 Hz.

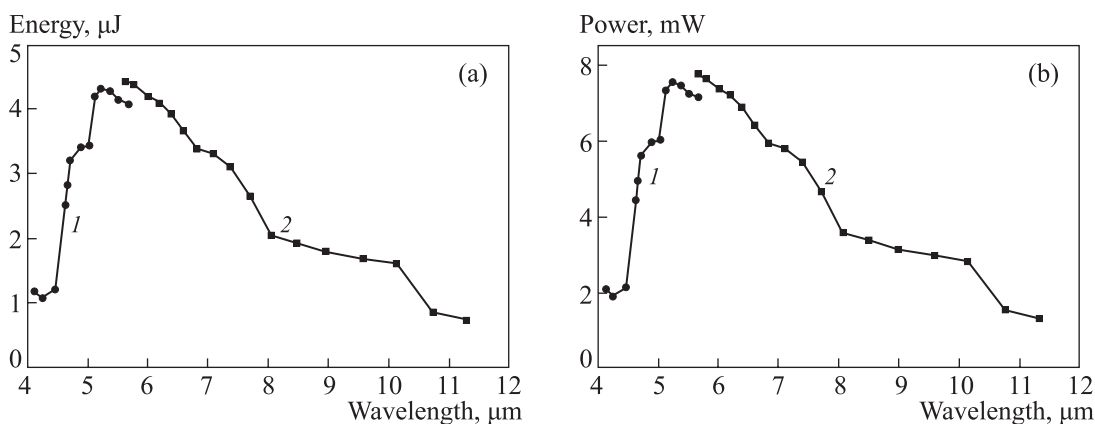


Fig. 4. Dependences of the (a) pulse energy and (b) average power on wavelength of OPO-2 for crystal #1 (1) and #2 (2); the pulse-repetition frequency is 1750 Hz.

was observed in the spectral range from 5 to 6 μm , whereas in the range of 9 to 11 μm the pulse energy decreased to 1 μJ .

Figure 4(b) presents a wavelength dependence of the average OPO-2 power. The pulse-repetition frequency was 1750 Hz. It can be seen that the wavelength dependence of the average power repeats the corresponding dependence of the OPO-2 pulse energy. The highest average OPO-2 power (about 8 mW) was obtained at the wavelength $\lambda = 5.2\text{--}6\ \mu\text{m}$. With an increase in wavelength, the average radiation power monotonically decreased to approximately 3 mW at the wavelength $\lambda = 10\ \mu\text{m}$.

The photoacoustic detector records absorption spectra of gas impurities entering the gas sample composition. A photodetector is used to normalize PAD signals with respect to the OPO radiation power. A reference cell is used to form spectral marks for the absorption spectra of marker gases (methane, acetone, N_2O , CF_4 , sulfur hexafluoride SF_6) when performing LaserBreeze self-testing and

determining the correctness of OPO-1 and OPO-2 spectral calibration.

3. STUDY OF THE ABSORPTION SPECTRA OF VOLATILE COMPOUNDS

Figure 5 presents room-air absorption spectra and reference-cell signals. The room-air temperature and relative humidity were 22°C and 46%, respectively.

The air absorption spectrum contains two strong absorption bands of water vapor (at 2.6 to 2.7 and 5.4 to 7.5 μm) and a carbon dioxide band (4.2 to 4.3 μm). The water vapor concentration in air was 8.95 g m^{-3} , or approximately 11140 ppm. The carbon dioxide concentration in pure air is about 330 ppm. The weak signal in the wavelength range from 3.2 to 3.3 μm can be attributed to hydrocarbons.

Figure 5(b) demonstrates the absorption spectra of VCs filling the gas-filled cell. The spectra contain characteristic absorption peaks of methane (wavelength 3.316 μm , concentration 10%), N_2O

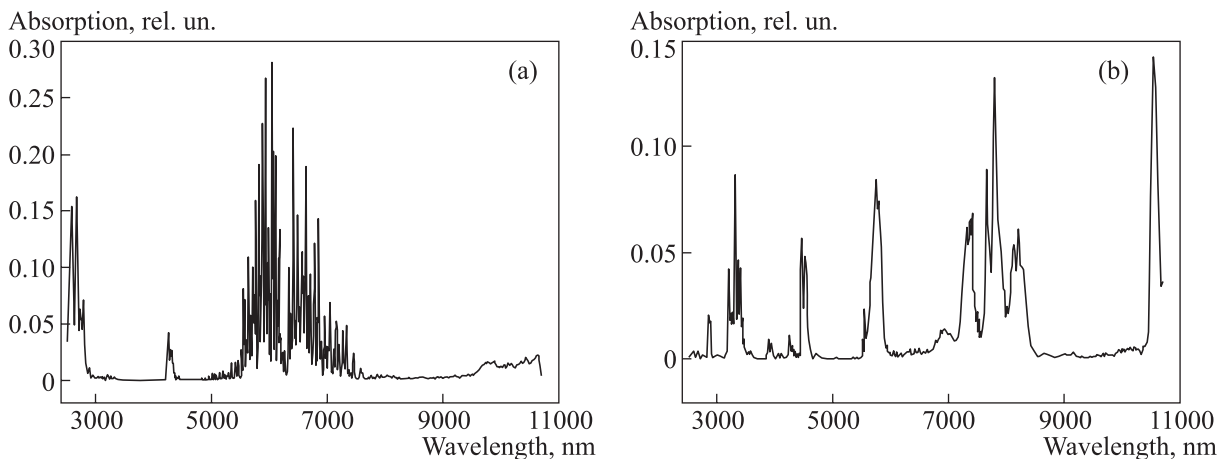


Fig. 5. Absorption spectra of (a) room air (temperature 22°C, relative humidity 46%) and (b) reference cell.

(4.468 μm , 5%), acetone (5.752 μm , 6%), CF_4 (7.796 μm , 2000 ppm), and SF_6 (10.55 μm , 2500 ppm).

It can be seen in Fig. 6 that methane (concentration 1000 ppm) has a strong narrow absorption line centered at 3.324 μm . One can also see absorption bands of water vapor (2.6 to 2.7 μm) and carbon dioxide (4.2 to 4.3 μm).

Figure 7 shows the absorption spectra of ethylene (concentration 1000 ppm) and acetylene (concentration 1000 ppm). Ethylene (Fig. 7(a)) has a narrow strong absorption peak at a wavelength of 10.53 μm , due to which it can easily be identified among other hydrocarbons. Acetylene (Fig. 7(b)) has an absorption band near 3.0 μm , which is shifted with respect to the absorption bands of methane, ethane, propane, etc., as a result of which it can also be identified among other hydrocarbons.

Figure 8(a) presents an absorption spectrum of carbon dioxide (concentration 2000 ppm). One can

see two peaks centered at 4.26 and 4.29 μm . The noisy spectral structure is explained by the strong absorption of atmospheric CO_2 .

Figure 8(b) shows absorption spectra of two carbon dioxide isotopes; the spectra were recorded for a test gas mixture containing 5000 ppm carbon dioxide,

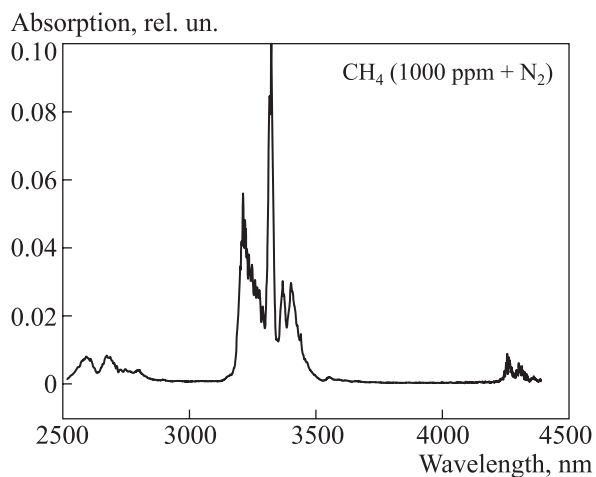


Fig. 6. Absorption spectrum of methane (CH_4).

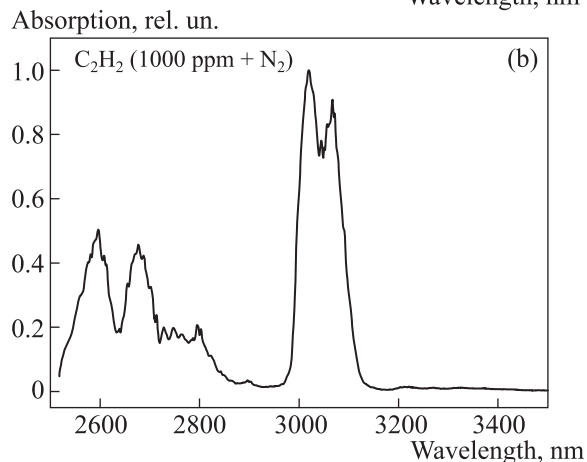
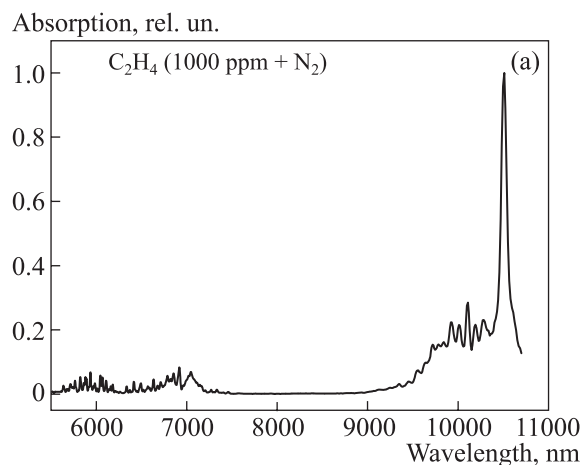


Fig. 7. Absorption spectra of (a) ethylene (C_2H_4) and (b) acetylene (C_2H_2).

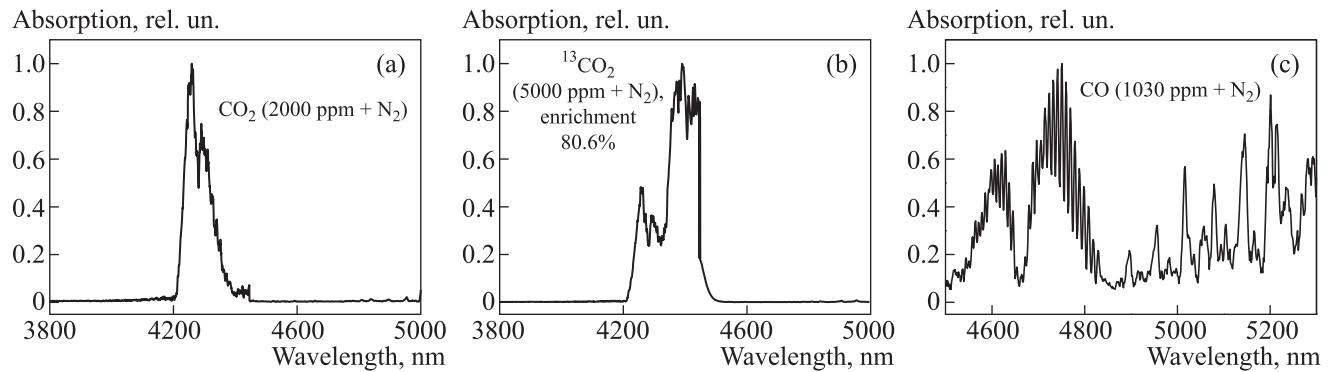


Fig. 8. Absorption spectra of (a) carbon dioxide (CO₂), (b) carbon dioxide isotope ¹³CO₂, and (c) carbon monoxide (CO).

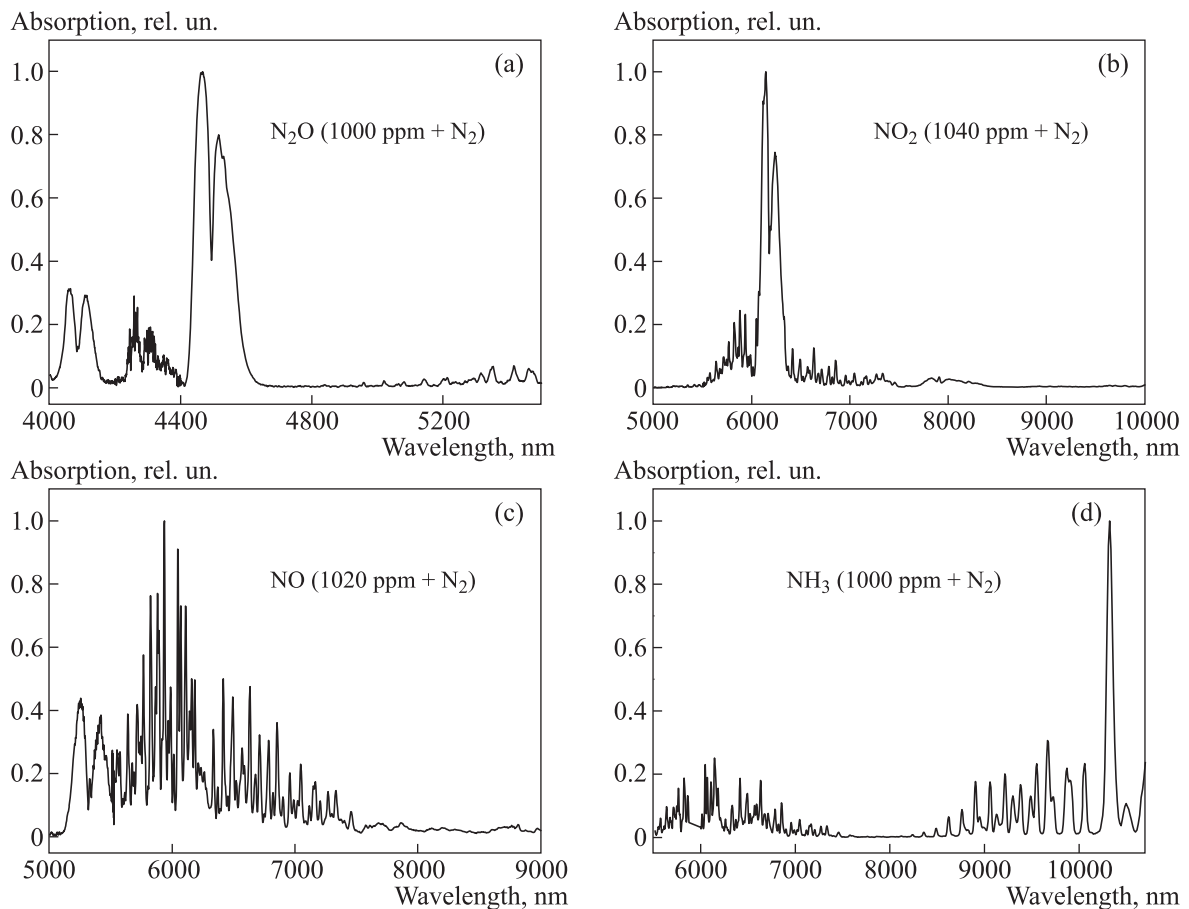


Fig. 9. Absorption spectra of (a) nitrous oxide (N₂O), (b) nitrogen dioxide (NO₂), (c) nitrogen monoxide (NO), and (d) ammonia (NH₃).

in which the content of ¹³CO₂ isotope was 80.6%. Two absorption peaks of conventional carbon dioxide (at 4.3 μm) and two absorption peaks of the ¹³CO₂ isotope (at 4.4 to 4.45 μm) can clearly be seen.

Figure 8(c) demonstrates an absorption spectrum of carbon monoxide (concentration 1030 ppm) in the range from 4.5 to 4.9 μm. One can clearly see two bands peaking at 4.63 and 4.75 μm. Each CO ab-

sorption band has a complex structure with many narrow peaks, which corresponds to the structure of transitions in the CO molecule. The absorption coefficient of carbon monoxide in the spectral range from 4.5 to 4.9 μm is rather low, so that even at a CO concentration of about 1000 ppm the intensity of CO absorption peaks is comparable with that of water vapor absorption lines, which are shifted to the right from the carbon monoxide absorption band. The

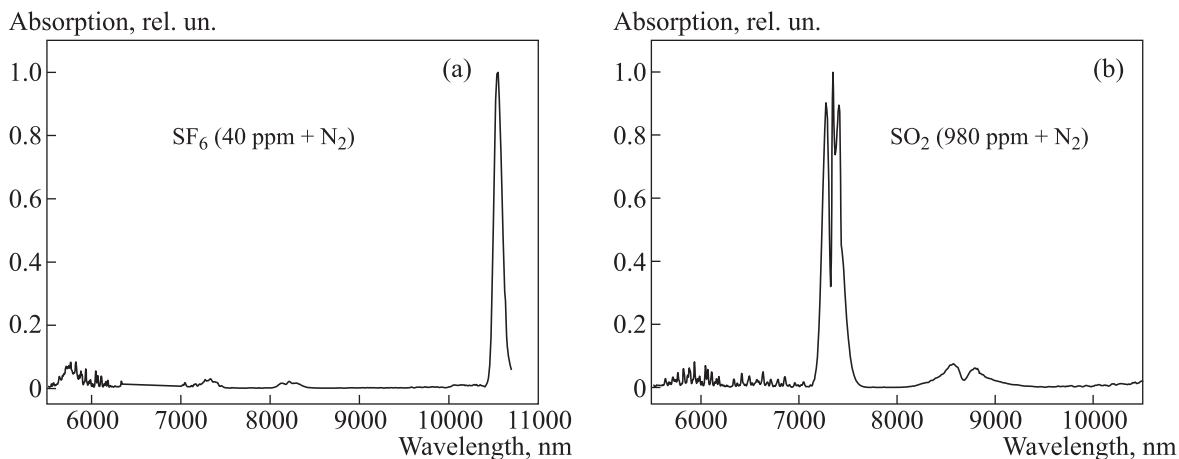


Fig. 10. Absorption spectra of (a) sulfur hexafluoride (SF₆) and (b) sulfur dioxide (SO₂).

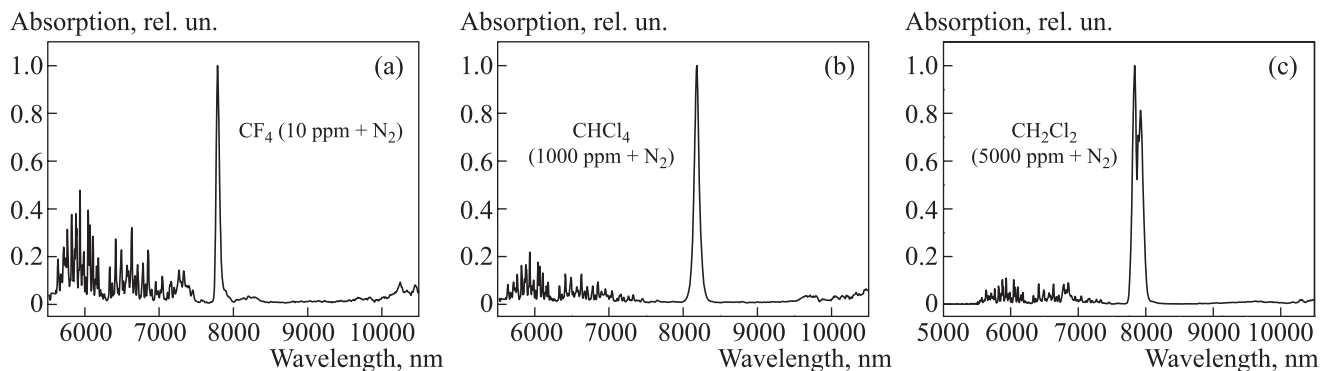


Fig. 11. Absorption spectra of (a) tetrafluoromethane (Chladon-14, CF₄), (b) trichloromethane (chloroform, CHCl₃), and (c) dichloromethane (CH₂Cl₂).

presence of the residual absorption spectrum of water vapor can be explained by contamination of the test gas mixture used.

Figure 9(a) shows an absorption spectrum of nitrous oxide (N₂O, concentration 1000 ppm). The strong absorption band of N₂O near 4.5 μm has two peaks, which are centered at 4.467 and 4.516 μm. In addition, there is a weaker N₂O absorption band near 4.1 μm.

Figure 9(b) shows an absorption spectrum of nitrogen dioxide (NO₂, concentration 1040 ppm) in the range from 4 to 11 μm. It contains a strong narrow absorption band, which is composed of two separate peaks peaking at 6.144 and 6.237 μm. These absorption peaks are imposed on the absorption spectrum of water vapor, which is depicted as a noisy background with frequent weak peaks.

Figure 9(c) presents an absorption spectrum of NO (concentration 1020 ppm) in the range from 4 to 11 μm, against the background of water vapor absorption. One can see two characteristic NO absorption peaks centered at 5.25 and 5.42 μm.

Figure 9(d) presents an absorption spectrum of NH₃ (concentration 1000 ppm) in the range from 5.5 to 11 μm. The strongest absorption peak is at 10.34 μm. The water vapor absorption band in the range from 5.5 to 7 μm can also be seen.

Figure 10(a) shows an absorption spectrum of SF₆ (concentration 40 ppm). Sulfur hexafluoride has a strong narrow absorption peak centered at 10.55 μm. The absorption coefficient of SF₆ at this wavelength is so high that very low concentrations (less than 0.1 ppm) of this gas can be detected. One can also see the residual absorption spectrum of water vapor in the range from 5.5 to 6.5 μm.

Figure 10(b) shows an absorption spectrum of SO₂ (concentration 980 ppm), which consists of three separate peaks. The central peak (at 7.346 μm) is the strongest one; it was used to identify SO₂ and measure its concentration.

Figure 11(a) shows an absorption spectrum of tetrafluoromethane (or Chladon-14) CF₄ (concentration 10 ppm). This compound has a strong single narrow absorption peak centered at 7.792 μm. The

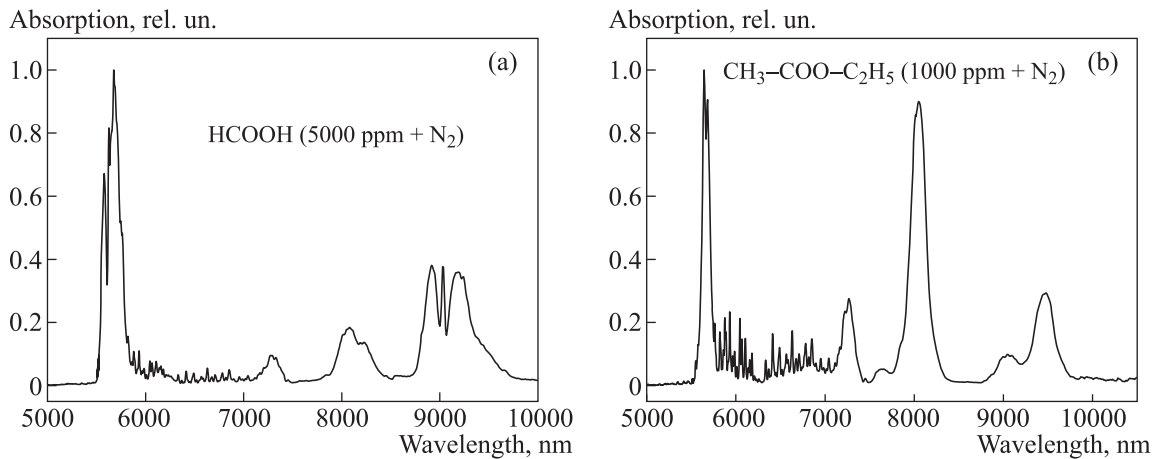


Fig. 12. Absorption spectra of (a) formic acid (HCOOH) and (b) ethyl acetate (CH₃-COO-C₂H₅).

Main technical characteristics

Parameters	Value
Concentration sensitivity	No worse than 1×10^{-3} ppm
Number of detected materials	No less than 20
Relative error in determining VC concentration	No more than 10 to 30%
Reliability and selectivity of VC identification	No less than 95%
Scanning range of OPO radiation wavelength	2.5 to 11 μm
Sample volume for detecting the VC composition and concentration	No more than 50 cm ³
Detection time for one VC in a sample	No more than 3 s
Detection time for 10 VCs in a sample	No more than 2 min
Time of analysis per sample	No more than 2 min

absorption coefficient of CF₄ at this wavelength is so high that allows for detecting this component in very low concentrations (less than 0.1 ppm). The plot contains also the residual absorption spectrum of water vapor in the range from 5.5 to 7 μm .

Figure 11(b) presents an absorption spectrum of trichloromethane (or chloroform) CHCl₃ (concentration 1000 ppm). This component contains a strong single narrow absorption peak centered at 8.195 μm ; it is used to identify chloroform and measure its concentration.

Figure 11(c) shows an absorption spectrum of dichloromethane CH₂Cl₂ (concentration 5000 ppm). This compound has a double absorption band with peaks at 7.838 and 7.926 μm . The 7.838- μm peak is used to identify dichloromethane.

Formic acid (Fig. 12(a)) has several absorption peaks of different intensities, which are centered at 5.715 (the strongest one), 8.195, and 8.924 μm .

Ethyl acetate (Fig. 12(b)) also has several absorption peaks of different intensities, with centers at 5.644, 8.060 μm , and some other wavelengths.

Figure 12 shows the absorption spectra of formic acid HCOOH (concentration 5000 ppm) and ethyl acetate CH₃-COO-C₂H₅ (concentration 1000 ppm).

4. CONCLUSIONS

We designed a gas analyzer for determining the composition of exhaled air by means of photoacoustic spectroscopy based on a broadband optical parametric oscillator and a photoacoustic detector, which provide a high-precision rapid analysis of the multicomponent composition of human exhaled air for dynamic estimation of the efficiency of treating bronchus and lung diseases. The main technical characteristics of the analyzer are listed in the table.

ACKNOWLEDGMENTS

The study was supported by the Federal Target Program "Investigation and Engineering in High-Priority Lines of Development of Science and Technology in Russia for 2007–2013" (State Contract No. 16.522.11.2001).

REFERENCES

1. J. Herrera, S. Krishnan, M. Zain, J. Greenberg, R.N. Cataneo, and M. Phillips, "Variations in Volatile Organic Compounds in the Breath of Normal Humans," *J. Chromatograph. B. Bio-Med. Sci. Appl.* **729**(1–2), 75 (1999).
2. E.B. Bukreeva, A.A. Bulanova, S.A. Tuzikov, E.L. Yumov, Yu.V. Kistenev, D.A. Kuz'min, and O.Yu. Nikiforova, "Specific Features of the Absorption Spectra of Air Exhaled by Patients with Noninfectious Chronic Diseases: Chronic Obstructive Disease and Lung Cancer," *Biotekhnosfera*. No. 3–4, 39 (2012).
3. V.I. Fyodorov, A.A. Karapuzikov, and M.K. Starikova, "Proteins, Peptides and Amino Acids As Markers of Bronchopulmonary Diseases," *Bull. Siberian Medicine*. **12**(6), 167 (2013).
4. Yu.V. Kistenev, K.I. Tchukikova, S.S. Gomboeva, and A.A. Karapuzikov, "Study Correlation of Absorption Spectra of Gas Excretions of Patients with Acute Viral Hepatitis, Obtained by Laser Opto-Acoustic Spectroscopy, with Blood Biochemical Parameters," *Med. Phys.* **4**(52), 32 (2011).
5. A. Miklós, P. Hess, and Z. Bozóki, "Application of Acoustic Resonators in Photoacoustic Trace Gas Analysis and Metrology," *Rev. Sci. Instrum.* **72**(4), 1937 (2001).
6. I.V. Sherstov, A.I. Karapuzikov, A.A. Karapuzikov, A.A. Boyko, M.K. Starikova, N.Yu. Dukhovnikova, V.N. Loconov, M.Yu. Shtyrov, I.B. Miroshnichenko, K.G. Zenov, M.B. Miroshnichenko, and D.B. Kolker, "PAD Spectrometer Based on Wide Tunable Optical Parametric Oscillator for Noninvasive Medical Diagnostics," *Opt. Photon. J.* **3**(2B), 43 (2013).
7. I.V. Sherstov, A.A. Karapuzikov, A.I. Karapuzikov, M.K. Starikova, D.A. Kashtanov, F.A. Mayorov, M.Yu. Shtyrov, A.A. Boyko, K.G. Zenov, M.B. Miroshnichenko, I.B. Miroshnichenko, N.Yu. Dukhovnikova, and D.B. Kolker, "PAD Spectrometer at 2.5–11 μm Based on Fan-Out PPLN and HgGa_2S_4 Optical Parametric Oscillator," in *Proceedings of the 6th International Symposium "Modern Problems of Laser Physics"* (Novosibirsk, 2013), p. 156.